Journal of Colloid and Interface Science 354 (2011) 691–699

Contents lists available at ScienceDirect

Journal of Colloid and Interface Science

www.elsevier.com/locate/jcis

Comparison of oleyl and elaidyl isomer surfactant–counterion systems in drag reduction, rheological properties and nanostructure

Yunying Qi [a,*], Ellina Kesselman [b], David J. Hart [c], Yeshayahu Talmon [b], Anthony Mateo [d], Jacques L. Zakin [a]

[a] Department of Chemical and Biomolecular Engineering, The Ohio State University, Columbus, OH 43210, USA
[b] Department of Chemical Engineering, Technion-Israel Institute of Technology, Haifa 32000, Israel
[c] Department of Chemistry, The Ohio State University, Columbus, OH 43210, USA
[d] Mapua Institute of Technology, Manila, Philippines

ARTICLE INFO

Article history:
Received 23 July 2010
Accepted 31 October 2010
Available online 8 November 2010

Keywords:
Drag reduction
Rheology
Nanostructure
NMR
Unsaturated quaternary ammonium cationic surfactant (oleyl vs. elaidyl)

ABSTRACT

Compared with quaternary ammonium cationic surfactants with saturated alkyl chains, quaternary ammonium cationic surfactants with one double-bond in their alkyl chains, when mixed with appropriate counterions (in certain molar concentration ratios, ξ), can reach much lower effective drag-reduction temperatures, while maintaining the upper drag-reduction temperature limit of the corresponding saturated drag reducing surfactant solutions. No previous study has compared the effects of cis- vs. trans-unsaturated alkyl hydrocarbon tail configurations (oleyl vs. elaidyl) trimethyl ammonium chloride cationic surfactants at different counterion/surfactant concentration ratios on micellar nanostructures, ^{1}H NMR spectra and on rheological and drag-reduction behavior of their solutions. Since neither pure oleyl (cis-) nor elaidyl (trans-) trimethyl ammonium chloride surfactants are commercially available, they were synthesized and their 5 mM solutions with NaSal counterion at concentrations of 5 mM, 7.5 mM and 12.5 mM were studied.

1. Introduction

Drag-reduction is a turbulent flow phenomenon by which small amounts of drag reducing additives (100–3000 ppm) can greatly reduce the friction factor of a turbulent flow [1]. Polymers and surfactants are the two most effective drag reducing additives. Great practical success with polymer solution additives was achieved in increasing the throughput in the 48-in. diameter Alyeska crude oil pipeline by up to 25% as early as 1979, and now polymer drag reducing additives are used extensively in oil pipelines all over the world to save pumping energy or increase throughput [2]. However, high molecular weight polymer molecules, when subjected to high shear or extensional stresses such as in pumps, contraction or expansion flows, will be broken up and the degradation is permanent. Thus, polymer drag reducing additives are only good for once-through systems.

In recent years, surfactant additives have been investigated as drag reducing additives because of their ability to repair their nanostructures after mechanical degradation. Surfactants are surface active amphiphiles with hydrophilic heads and hydrophobic tails which aggregate in water above a critical micelle concentration (CMC) to form micelles to avoid unfavorable interactions between their hydrophobic tails and water. Micelle nanostructures can be spherical, rodlike, threadlike, etc. Micelles are in a state of thermodynamic equilibrium with the solvent and are perpetually broken and reformed under Brownian fluctuation [3]. This leads to a broad and dynamic distribution of micelle lengths which, as proposed by Cates and Turner can change under an imposed shear or extensional flow [4].

Gyr and Bewersdorff reviewed the surfactant drag reduction literature and concluded that threadlike micelles are responsible for the drag reducing ability of surfactant solutions [5]. They also reviewed the fluid mechanics and rheological behaviors of drag reducing surfactant systems. They noted that SANS measurements on flowing drag reducing surfactant solutions showed that micelles are oriented with their long axes parallel to the flow direction. Velocity fluctuations perpendicular to the flow (normal to the wall) are greatly reduced compared to those of pure solvent at the same flow rate while axial velocity fluctuations remain large. The time averaged product of these two velocity fluctuations at any point in the turbulent flow are called the Reynolds stress which is the major component of the local stress in the turbulent region away from the wall. In strongly drag reducing flows these two velocity fluctuations are nearly completely decoupled [6,7] and the resultant lowered Reynolds stress in the turbulent core, along with lower velocity gradient in the near wall region result in large decreases in drag (drag reduction). It was hypothesized by Gyr and Bewerdorff [5] and by Hu and Matthys [8] that for threadlike micelles aligned with the flow, elongational flow is more effective in

* Corresponding author.
E-mail address: yunying.qi@gmail.com (Y. Qi).

0021-9797/$ - see front matter © 2010 Elsevier Inc. All rights reserved.
doi:10.1016/j.jcis.2010.10.067

producing micelle growth than shear flow as it favors side to side collision between micelles causing the micelles to grow in size after collision through fusion.

Because of the self-assembling nature of surfactant micelles, mechanically degraded nanostructures are recoverable and they are also temperature reversible. These properties make them very promising for use in recirculation systems such as in recirculating district heating and cooling systems to save pumping energy [9].

Quaternary ammonium cationic surfactants are very effective drag reducing additives. Their effective drag reducing temperature ranges and wall shear stress limits depend on the surfactant and the counterion chemical structures, their concentrations and their molar ratios. The lower drag-reduction temperature limit is determined by the solubility of the surfactant, while the upper drag-reduction temperature limit is determined by breakdown of the micelle nanostructure. Rose and Foster [10] found that when the length of surfactant alkyl chain increases, the upper drag-reduction temperature of surfactant solutions increases. However, it was found that surfactants with saturated alkyl chain lengths of more than 16 carbon numbers are insoluble at low temperatures, which limits their low temperature drag-reduction range.

To lower this lower drag-reduction temperature limit, Rose and Foster [10] suggested incorporating a double-bond in the alkyl chain, or replacing two or three methyl groups with hydroxyethyl groups in the quaternary ammonium cationic surfactant headgroup. Such surfactants are more soluble at low temperatures, while maintaining the high critical temperatures and Reynolds numbers of their saturated alkyltrimethylammonium counterparts. The most important consequence of unsaturation is to lower the lowest temperature at which fluid states may exist [11].

Lu et al. [12] observed that a commercial surfactant derived from soya oil (Arquad 5–50 – soya N $(CH_3)_3Cl$) with sodium salicylate counterion was a good drag reducing additive but, unlike most effective drag reducing additives, it showed no non-zero first normal stress (N_1) and essentially no recoil behavior. The manufacturer, Akzo Nobel, indicated that the composition of the soya was 17% C_{16} and 81% C_{18} chains, 70% of which were unsaturated [12]. Later it was disclosed that the soya purification process gave a mixture of cis and trans chains in about equal quantities [13]. For some time we have been perplexed by the absence of viscoelastic behavior in this drag reducing surfactant system. Since all other cationic/counterion drag reducing additive containing unsaturated chains reported in the literature have the natural cis configuration, we undertook a study of the difference between cis (oleyl) and trans (elaidyl) trimethyl ammonium chloride surfactant, which we synthesized to determine if elaidyl might be responsible for this unusual behavior and to compare their micelle structures, rheological behavior and drag reducing abilities.

The two forms of one double-bond unsaturation, cis- and trans-, are shown in Fig. 1. The cis-double-bond has both groups on the same side of the double-bond while the trans-double-bond has them on opposite sides of the double-bond. The differences in the steric hydrocarbon chain configurations of these two isomers would be expected to affect the micelle nanostructures, the rheological behaviors and the drag-reduction abilities of corresponding drag reducing surfactant solutions but to date no measurements comparing them have been made.

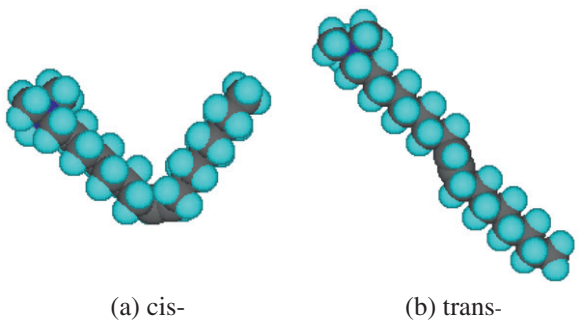

Fig. 1. Schematic view of cis- and trans-forms of surfactant hydrocarbon chains.

According to Israelachvili [14], the geometrical factors of the surfactant molecules determine the most favored structures of micelles. The geometric factors of the surfactant molecules are usually described by the surfactant molecular packing parameter, $p = \frac{v}{a_0 l_c}$, in which v, is the hydrophobic chain volume, a_0, is the effective surface area the hydrophilic headgroup occupies at the micelle hydrophobic/hydrophilic interface and l_c is the critical hydrophobic chain length which defines how far the chain can extend. In dilute surfactant solutions, spherical micelles form when $p < \frac{1}{3}$, while for rodlike micelles, $\frac{1}{3} < p < \frac{1}{2}$, and for vesicles, $\frac{1}{2} < p < 1$.

Israelachvili pointed out that introduction of unsaturation reduces the critical chain length and therefore increases the packing parameter of the surfactant molecules which favors micelle chain growth. As can be seen in Fig. 1, the kink in the hydrocarbon chain of the cis double-bond increases the volume occupied by the hydrocarbon tail giving larger packing parameter which results in a large end cap energy, E_c, (the energy related to the surfactant packing near the cylinder end-caps), and favors micelle growth [14]. The cis configuration, therefore might be expected to have larger micelles, vesicles and ultimately invert structures.

According to Laughlin [11], the elaidyl, with a trans double-bond, has a linear shape which is not grossly different from that of a saturated chain and also results in a lower temperature for the fluid state (Krafft point). As can be seen from Fig. 1, replacement of a saturated bond with a trans-double-bond in the hydrocarbon chain of a surfactant molecule is not as effective in increasing the packing parameter of a surfactant molecule as the cis-double-bond.

To investigate the relations of the two surfactant configurations on drag-reduction abilities, rheological properties and surfactant nanostructures, we measured those properties along with cryo-TEM and ^{1}H NMR of elaidyl trimethyl ammonium chloride (trans-) (5 mM) and oleyl trimethyl ammonium chloride (cis-) (5 mM) with the counterion sodium salicylate (NaSal) at concentrations of 5 mM, 7 mM and 12.5 mM.

2. Experimental methods

2.1. Materials

Since the two isomeric alkyltrimethyl ammonium chloride cationic surfactants tested, elaidyl trimethylammonium chloride and oleyl trimethylammonium chloride, were not commercially available, they were synthesized as follows. The cis- and (trans-9-octadecen-1-ols were first produced by reduction of oleic acid and elaidic acid with lithium aluminum hydride. Upon reaction with triphenylphosphine in carbon tetrachloride at reflux, these alcohols were then converted to cis- and trans-9-octadecenyl chlorides. Reaction of the chlorides with ethanolic trimethylamine in a pressure tube at 95 °C gave the required surfactants after purification by trituration with diethyl ether. We characterized each surfactant by ^{1}H and ^{13}C NMR spectroscopy and mass spectrometry and found them free of contaminants (no trans in the cis and no cis in the trans), with the exception of the presence of trace amounts of tetramethylammonium chloride.

Sodium salicylate, purchased from Aldrich Chemical Co. (99%), was used as the counterion. Concentrations of the surfactants were 5 mM and counterion concentrations were 5 mM, 7.5 mM and

12.5 mM. All solutions were clear at room temperature except the oleyl solution with 12.5 mM of sodium salicylate which was turbid.

2.2. Drag-reduction measurements

Turbulent drag-reduction experiments were conducted in a recirculation system with a 1.22 m long, 6 mm inner diameter stainless steel tube test section. The temperature of the systems was controlled by a heater and a cooling heat exchanger which allowed experiments to be run from 2 °C to 150 °C. Detailed description of the system can be found in Lu (1997) [15]. The data are reported as% drag-reduction = $\{[(\Delta P/L)_{water} - (\Delta P/L)]_{solution}]/(\Delta P/L)_{water}\}100$, where $\Delta P/L$ is the measured pressure gradient. Temperatures were controlled to ±0.3 °C and solvent Reynolds numbers ranged from 15,000 to about 60,000 at the lowest temperature and from ≈60,000 to 200,000 at the highest temperature.

2.3. Rheological measurements

2.3.1. Shear viscosity

Shear viscosity measurements were carried out with a Rheometrics RFSII Couette rheometer. The Couette cell had a cup diameter of 34 mm, and bob diameter of 32 mm, giving a fixed gap of 1 mm. The bob length was 32 mm. The experiments were run at room temperature (≈22 °C). To make sure the viscosities reach equilibrium at each shear rate, the solutions were sheared for 60 s at each shear rate before taking the data. At each shear rate, the shear viscosity was calculated from the average of clockwise rotation followed by counter clockwise rotation measurements.

2.3.2. First normal stress difference

First normal stress differences of the solutions were measured in a Rheometric Scientific Inc. RMS-800 rheometer with a cone-and plate fixture with a diameter of 50 mm and cone angle of 0.04 radians. The experiments were conducted at room temperature which is around 20 ± 2 °C. The shear rate range tested was from 25 s^{-1} to 800 s^{-1} with the lowest shear rate limited by the low sensitivity of the transducer, and the maximum shear rate limited by foaming of the surfactant solutions.

All first normal stress difference results measured with the RMS-800 rheometer were corrected for inertial effects using the following equation given by Macosko [16].

$$N_{1\ corrected} = N_{1\ reading} + 0.15\rho\Omega^2 R_p^2 \quad (1)$$

where ρ is solution density, Ω is angular velocity and R_p is cone radius. Because the inertial force is in the opposite direction to the normal force, the correction term, $0.15\rho\Omega^2 R_p^2$, should be added to the rheometer output, giving an increase in $N_{1\ corrected}$.

2.3.3. Apparent extensional viscosity

Apparent extensional viscosities were measured using a Rheometric Scientific, Inc. RFX instrument, which employs two opposed nozzles to generate an extensional flow. By using two syringe pumps connected to the two nozzles, solutions were sucked into the nozzles to generate an extensional flow between them. With three sets of nozzles of diameters of 0.5 mm, 1 mm and 2 mm, respectively and the separation gap between the two jets set equal to the nozzle diameter, extensional rates from 20 s^{-1} to 10,000 s^{-1} were covered. During experiments, the two nozzles were immersed in the test solutions which were held in a 250 ml jacketed beaker. The beaker was connected to a bath system allowing temperature control to within ±0.5 °C of the desired temperature. Detailed description and analysis of the instrument can be found in Macosko [16]. The reported results are the average of three repeated experiments. The extensional viscosity measured in the RFX is not the "true" extensional viscosity of the liquid, however. It includes contributions from dynamic pressure, shear on the nozzles and liquid inertia [16]. The measured property is therefore an apparent extensional viscosity; the magnitude of the extensional viscosity is larger than the measured quantity.

2.3.4. Cryo-TEM

To take cryo-TEM images of drag reducing surfactant solutions, the samples were prepared in a controlled temperature and humidity chamber. When preparing samples, a small drop of the studied solution is applied on a perforated carbon film supported by an electron microscope grid. The drop is then blotted to a very thin liquid film, and is rapidly plunged into liquid ethane at its freezing point (~90 K) to vitrify the liquid [17,18]. Images of the vitrified samples were then recorded at nominal objective lens under focus of 1–2 μm with a Philips CM120 transmission electron microscope operated at 120 kV, using an Oxford CT 3500 cooling holder operated at about −180 °C.

The whole process is designed to avoid water crystallization so that the nanostructure is not disturbed and the images obtained reflect the true structures in the original solutions. However, in the blotting step to form a thin film on the grid, the samples experience very high shear rates which may cause nanostructure transitions [18]. In addition, different portions of the film may be subjected to different intensities of shear during blotting and as a result, the vitrified film of the sample suspended over the polymer grid has a thickness distribution after blotting ranging from 200 to 400 nm near the edge and 10 nm at the thinner part. The thicker part, therefore, appears darker in the final image while the thinnest part, where the density of the micelles or vesicles is relatively small, is brighter. It should be noted that the shear imposed in blotting is large and induces shear induced structures (SIS).

2.3.5. NMR measurements

NMR measurements were performed using a Bruker AM-600 600 MHz (14.14 T) NMR spectrometer. All samples were prepared with D_2O and run in standard 5 mm NMR tubes.

3. Results and discussions

3.1. Drag-reduction

Fig. 2 shows the drag-reduction results of the elaidyl trimethyl ammonium chloride/NaSal (5 mM/12.5 mM) system. The effective drag-reduction temperature range is 4–80 °C for this solution, with maximum reduction of drag of 70%. The effective drag-reduction temperature range is defined as the temperature-range where the

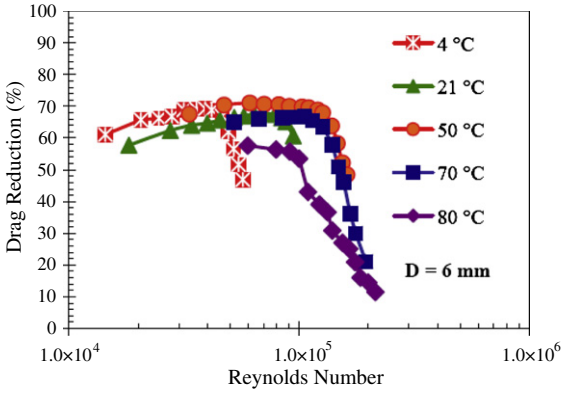

Fig. 2. Drag reduction results of elaidyl trimethyl ammonium chloride/NaSal (5 mM/12.5 mM) system.

Table 1
Effective drag reduction temperature ranges and critical wall shear stresses of elaidyl trimethyl ammonium chloride (5 mM)/NaSal and oleyl trimethyl ammonium chloride (5 mM)/NaSal solutions at room temperature (22 °C) with three different counterion/surfactant molar concentration ratios, ξ = 1.0, 1.5 and 2.5.

	ξ = 1.0		ξ = 1.5		ξ = 2.5	
	Effective temperature range (°C)	Critical wall shear stress (Pa) at 22 °C	Effective temperature range (°C)	Critical wall shear stress (Pa) at 22 °C	Effective temperature range (°C)	Critical wall shear stress (Pa) at 22 °C
Oleyl	21–60	30	4 to ~60	160	50–80	N/A
Elaidyl	21–60	19	5 to ~65	100	4 to ~80	290

drag-reduction is greater than 50%. Drag-reduction results for the other systems studied were qualitatively similar except for the oleyl surfactant at counterion to surfactant molar ratios ξ, which was not soluble below 50 °C (ξ = counterion/surfactant molar ratio). A summary of the effective drag-reduction temperature ranges of the solutions, and the solution critical wall shear stresses (at which drag-reduction percentage drops to 50% after passing the peak) at room temperature (around 22 °C), at ξ values of 1.0, 1.5 and 2.5 are shown in Table 1.

As can be seen from Table 1, at counterion concentration ratios ξ = 1 and ξ = 1.5, the effective drag-reduction temperature ranges of oleyl and elaidyl surfactant solutions are about the same. However, the critical wall shear stresses of oleyl solutions are about 60% higher than those of the elaidyl solutions, indicating that the wormlike micelles of the elaidyl surfactant solutions responsible for drag-reduction are more susceptible to break up by shear than those of the oleyl solutions. With further increase of counterion/surfactant ratio to ξ = 2.5, the oleyl surfactant solution was insoluble up to a temperature of 50 °C, while the elaidyl (ξ = 2.5) solution shows very good drag-reduction down to 4 °C. The upper drag-reduction temperature limits of both ξ = 2.5 solutions are about 80 °C.

From Table 1, it can also be seen that, except for oleyl at ξ = 2.5, as the counterion/surfactant concentration ratio increases, the effective drag-reduction temperature ranges of the surfactant solutions are extended, and the critical wall shear stresses of the surfactant solutions also increase significantly. Thus the addition of excess counterion increases the resistance of the surfactant nanostructures of the solutions to shear presumably because of strong interaction between micelles as the surface charges are dispersed (see cryo-TEM below). Similar results were reported earlier by Rose and Foster [10].

3.2. Cryo-TEM images

Cryo-TEM images of oleyl and elaidyl drag reducing surfactant solutions with different counterion/surfactant concentration ratios, ξ, are shown in Figs. 3 and 4. Both the ξ = 1.0 (Fig. 3a) and ξ = 1.5 oleyl (Fig. 3b) surfactant solutions at 25 °C have threadlike network nanostructures. However, since increasing counterion

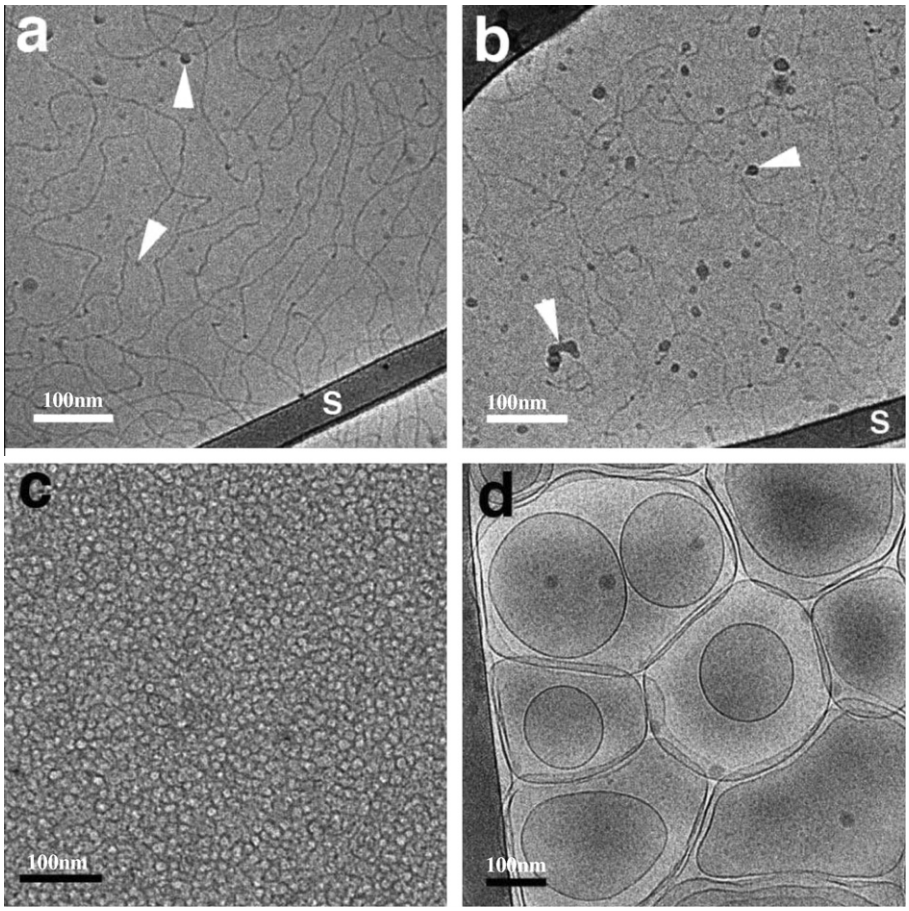

Fig. 3. Cryo-TEM images of oleyl trimethyl ammonium chloride with (a) 5 mM NaSal at 25 °C; (b) 7.5 mM NaSal at 25 °C; (c) 12.5 mM NaSal at 25 °C; (d) 12.5 mM NaSal at 50 °C. Arrows point to specs of frost and 'S' denotes the support film.

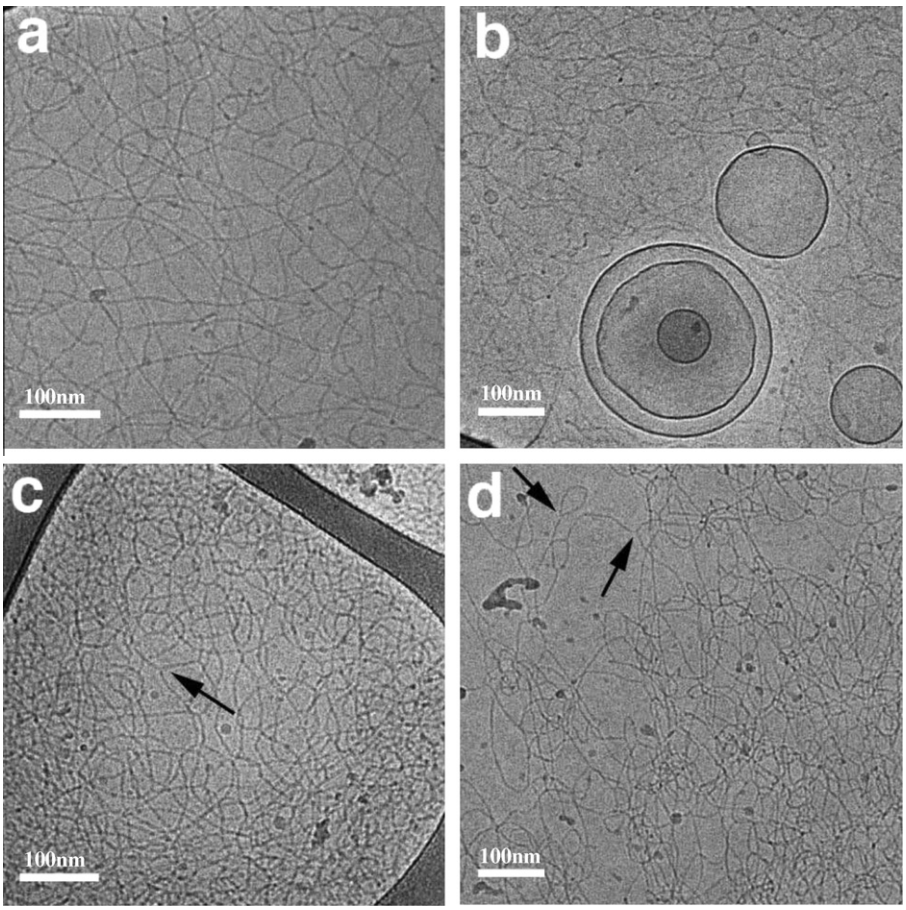

Fig. 4. Cryo-TEM images of elaidyl trimethyl ammonium chloride with (a) 5 mM NaSal at 25 °C; (b) 7.5 mM NaSal at 25 °C; (c) 12.5 mM NaSal at 25 °C; (d) 12.5 mM NaSal at 50 °C. Arrows point to branching points.

concentration not only decreases the electrostatic repulsive interactions between the micelles, but also decreases the self-repulsion of a threadlike micelle along its length [20–26], the threadlike micelles in the oleyl ($\xi = 1.5$) solution are expected to be longer and more flexible with shorter persistence lengths than those in the oleyl ($\xi = 1.0$) solution. While cryo-TEM is an excellent tool to determine the morphology of the aggregate, quantitative aspects have to be obtained from other techniques, differences in the flexibility and length of the micelles are difficult to discern from their cryo-TEM images, which are only single snapshots of their nanostructure. The decreased electrostatic repulsive forces between oleyl micelles at $\xi = 1.5$ also increases the interactions between the micelles, so the micelles in the oleyl ($\xi = 1.5$) solution are expected to be closer to each other than in the oleyl ($\xi = 1.0$) solution. Both of these effects contribute to the higher critical wall shear stresses of the $\xi = 1.5$ solution than the $\xi = 1.0$ solution observed in the room temperature drag-reduction experiments (Table 1).

It should be noted that at ξ values between 1.0 and 1.5 (see NMR section and Fig. 8b) the oleyl surfactant phase separates presumably going from a soluble dilute phase to an insoluble semi-dilute phase. Under shear in the rheological measurements, in turbulent flow and in the cryo-TEM blotting step, however, the $\xi = 1.5$ surfactant system is solubilized.

The oleyl ($\xi = 2.5$) solution is phase separated up to 50 °C due to the very close packing of the surfactant molecules. The phase-separated oleyl ($\xi = 2.5$) surfactant solution's cryo-TEM image at 25 °C shows a complicated, dense network of threadlike micelles in the denser, higher concentration phase (Fig. 3c). As the temperature increases to 50 °C, vesicles are formed in this solution as shown in Fig. 3d. While threadlike micelles are usually regarded as necessary requirements for surfactant solutions to be drag reducing [5] but the 50 °C system is drag reducing. The presence of vesicles and the absence of thread like micelles in the oleyl ($\xi = 2.5$) drag reducing system at 50 °C may be explained by the results of Zheng et al. [19]. They investigated the nanostructure transitions induced during specimen preparation of a drag reducing surfactant solution, Arquad 16-50/3-methylsalicylate (5 mM/5 mM). After vitrifying the blotted samples at times ranging from 0.5 to 120 s, they found that vesicles were transformed into threadlike micelles by the shearing action of the blotting during specimen preparation, but they quickly relaxed back to vesicles with time, giving structures similar to those in Fig. 3d in less than 30 s.

Threadlike micelles are found in the elaidyl solutions at all three counterion/surfactant concentration ratios: $\xi = 1.0$, 1.5 and 2.5 at 25 °C. An entangled threadlike micellar network is observed in the $\xi = 1.0$ solution (Fig. 4a). When the counterion/surfactant concentration ratio is increased to $\xi = 1.5$, longer and more flexible threadlike micelles are formed, with stronger interactions between the micelles. That leads to the higher critical wall shear stress of the $\xi = 1.5$ solution compared with the $\xi = 1.0$ solution in drag-reduction measurements (Table 1). Some vesicles are observed in a "sea" of entangled threadlike micelles. Similar to the oleyl ($\xi = 2.5$) solution at 50 °C, it is postulated that the vesicles in the elaidyl ($\xi = 1.5$) solution at 25 °C (Fig. 4b) transform to threadlike micelles when subjected to shear.

With further increase of counterion/surfactant ratio to $\xi = 2.5$, a number of branched micelles can be seen in the elaidyl system (Fig. 4c), one of which is noted by an arrow. Little difference is

observed in the nanostructure of elaidyl ($\xi = 2.5$) solution as temperature increases from 25 °C (Fig. 4c) to 50 °C (Fig. 4d). Micellar systems with branches, such as those seen in Fig. 4c for the elaidyl ($\xi = 2.5$) solution are usually found in surfactant solutions with high counterion concentration or high pH, where the repulsions between headgroups are well-screened [23,26–30]. High critical wall shear stress is associated with branched networks [31,32] as was observed with this system (Table 1).

Branch formation can be explained as follows. For conventional surfactants, the free energy cost for forming a cross-link branching point is much higher than for forming a hemispherical end-cap terminating a cylindrical micelle. This is because the surfactant layer at the junction of two branches is concave, whereas it is convex at the end of the cylindrical part of the micelle with the layer curvature essentially the same as the spontaneous curvature of the cylindrical part. With increasing counterion concentration, end cap energy (the energy that is related to the surfactant packing near the cylinder end-caps) of threadlike micelles increases due to decreased electrostatic repulsion energy which leads to an increase in the average micellar length [20]. At very high counterion concentration, any change of conditions (counterion concentration; alcohol concentration, etc.) that increases the end cap (positively curved) energy should decrease the energy required to form a negatively curved crosslinking point, and hence favor inter-micellar connections (branching) [26,33–40].

While branching (junction formation) is generally energetically unfavorable at high concentrations, it may be favored [as a way to get rid of energetically unfavorable end-caps] on enthropic grounds due to inter-micellar [excluded volume] interactions. Thus, the relative magnitude of the energy for formation of a junction and the end cap excess energy determine the conditions favorable for formation of branches [32]. As seen in Table 1, the elaidyl ($\xi = 2.5$) solution with branched threadlike micelles exhibits very high critical wall shear stress because of the strong interactions between the micelles and the branched structures. The formation of branches also reduces viscosity [25,32]. The decrease in viscosity associated with branched micelles occurs because the cross [36] in the multi-connected networks can slide along the micelles, serving as stress release points [34,41].

As mentioned earlier, from cryo-TEM images, it is difficult to determine the differences in the flexibility, length of the micelles and the interactions between the micelles since each image is only a snapshot of the nanostructure at a single moment, which cannot provide much quantitative information about the threadlike micelles. In addition, the entanglement of the threadlike micelles observed in the cryo-TEM images of the solutions sometimes can be misleading, because cryo-TEM images give a 2-D representation of a 3-D object [18,42] and because the depth of field of the TEM is larger than the specimen thickness.

3.3. Rheological behavior

3.3.1. Shear viscosity

Shear viscosities of the oleyl and elaidyl solutions with different counterion/surfactant concentration ratios, ξ, at room temperature are shown in Fig. 5. The low shear rate (<1 s^{-1}) shear viscosities of the oleyl solution ($\xi = 1.0$) are much larger than those of the $\xi = 1.0$ elaidyl solution. However, as counterion/surfactant concentration ratio increases to 1.5, the low shear rate shear viscosities of the elaidyl solution increase to about 10 times that of the elaidyl ($\xi = 1.0$) solution, while the shear viscosities of the $\xi = 1.5$ oleyl solution at low shear rates decrease to about 1/10 that of the oleyl ($\xi = 1.0$) solution (Fig. 5). Thus, the low shear rate shear viscosities of the elaidyl solutions at $\xi = 1.5$ are much larger than those of the $\xi = 1.5$ oleyl solution. With further increase of counterion/surfactant concentration ratio, the oleyl ($\xi = 2.5$) solution becomes insoluble,

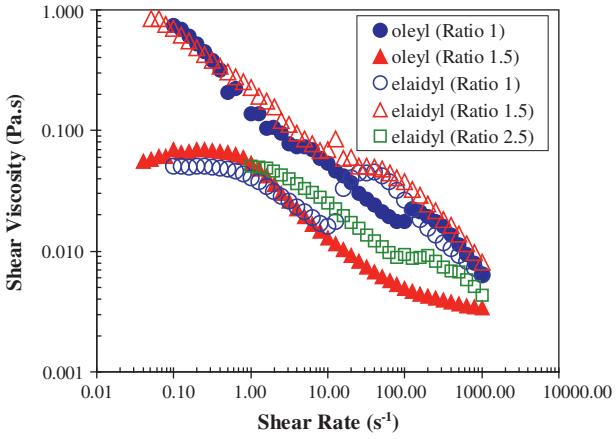

Fig. 5. Shear viscosities of oleyl and elaidyl (5 mM)/sodium salicylate (5 mM; 7.5 mM and 12.5 mM) solutions at room temperature. Note: oleyl ($\xi = 2.5$) solution is insoluble until 50 °C.

and the shear viscosities of the branched elaidyl ($\xi = 2.5$) solution are low at high shear rates because the junctions provide a means to relieve stress [34,41]. Comparing Fig. 5 and Table 1, it can be seen that there is no direct relation between shear viscosity and drag-reduction effectiveness of the surfactant solutions.

All the solutions tested show shear-thinning behavior above a shear rate of 1 s^{-1} or lower. Elaidyl at $\xi = 1.0$ and 2.5 and oleyl at $\xi = 1.5$ are Newtonian at low shear rates. Elaidyl at $\xi = 1.0$, which has threadlike micelles, shows a large shear thickening effect starting at about 10 s^{-1}. Interestingly, both the oleyl ($\xi = 1.0$) solution with threadlike micelles and the elaidyl ($\xi = 1.5$) solution with mixture of vesicles and threadlike micelles which have the highest viscosities show only modest shear thickening peaks in their shear viscosity vs. shear rate plots due to formation of shear induced structures (SIS). No SIS is observed in the oleyl ($\xi = 1.5$) solution, with very long and flexible threadlike micelles, in the shear rate range tested. The shear behavior of elaidyl ($\xi = 2.5$) solution with a number of branched threadlike micelles is similar to that of oleyl ($\xi = 1.5$) at shear rates below 100 s^{-1}. However, beginning at a shear rate near 100 s^{-1}, a small SIS is observed in the shear viscosity curve of this solution. Many researchers [42–47] have proposed theoretically that shear thickening behavior of surfactant solution with threadlike micelles is caused by enhanced rates of collision and collinear fusion between aligned and extended threadlike micelles in the flow field. The pattern of influence of ξ on SIS is not clear but high ξ, which favors branching, appears to delay SIS to higher shear rates as also reported by Qi and Zakin [27].

3.3.2. First normal stress difference (N_1)

Viscoelastic properties of surfactant solutions are usually exhibited in the form of non-zero first normal stress difference (N_1), quick recoil and stress overshoot and are generally accompanied by shear induced structure (SIS) [25]. The first normal stress differences of surfactant solutions oleyl and elaidyl with different counterion/surfactant concentration ratios at room temperature are shown in Fig. 6. The oleyl ($\xi = 1.5$) solution with very long and flexible threadlike micelles had zero and negative N_1. (Negative values at high shear rate are due to strong inertial effects in the measurements.) The other four solutions with threadlike networks (oleyl ($\xi = 1.0$) and elaidyl ($\xi = 1.0$)), branched threadlike micelle network (elaidyl ($\xi = 2.5$)) or mixtures of threadlike micelles and vesicles (elaidyl ($\xi = 1.5$)) all exhibited strong viscoelasticity with high first normal stress differences in the 20–800 s^{-1} shear rate range tested. These results correspond well to the SIS in the shear viscosity vs. shear rate plot in Fig. 5 where no SIS was observed with the oleyl

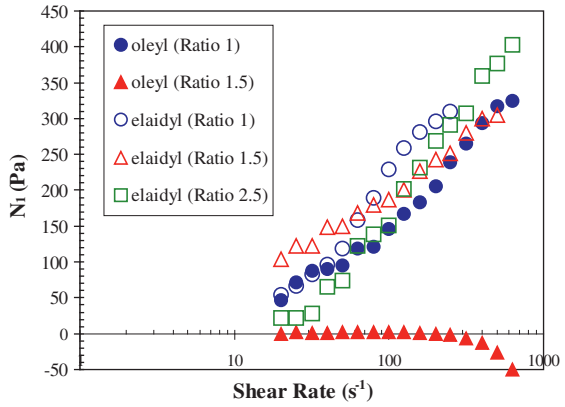

Fig. 6. First normal stress differences of oleyl and elaidyl (5 mM)/sodium salicylate (5 mM; 7.5 mM and 12.5 mM) solutions at room temperature. Note: oleyl ($\xi = 2.5$) solution is insoluble until 50 °C.

($\xi = 1.5$) solution while the other four solutions show various levels of SIS. Nowak [48] noted the occurrence of elastic effects (N_1) coinciding with increase in shear viscosity and Qi et al. [49] noted that non-zero N_1 was initiated at shear rates near those for initiation of SIS. Here they are generally lower. Nevertheless, the oleyl ($\xi = 1.5$) solution with no SIS observed in the shear rate range of 0.02–1000 s^{-1} and zero or negative N_1 in the shear rate range of 20–800 s^{-1}, has good drag-reduction effectiveness over a reasonably wide temperature range, 5 to ~65 °C and a high critical wall shear stress, which illustrates that conventional viscoelastic behavior is not a requirement for good drag reduction, as previously noted by Lu et al. [12].

Butler et al. [20] and Hamilton et al. [21] pointed out that for surfactant solutions with very flexible threadlike micelles (small micellar charge density, many curves between entangling points) such as the oleyl ($\xi = 1.5$) solution, there are two steps involved in the shearing alignment process of threadlike micelles along the flow direction. The first step is a local deformation (stretching) of the network resulting in alignment of micellar segments over a length scale of roughly the distance between entanglement points. The effect of this alignment process on the rheological properties of the solution at a given shear rate depends strongly on the persistence length of the threadlike micelles. The shorter the persistence length, the more flexible the threadlike micelles, with more curves along the micelle segment between two entangling points requiring higher shear to align the micelle segments between two entangling points along the flow direction. Qi et al. [49] observed that before the second step begins in a surfactant solution, zero first normal stress difference is observed.

The second step is the large scale disentanglement and alignment of the individual threadlike micelles along the flow direction. When this step starts, the solution exhibits non-zero N_1 values. For solutions with small electrostatic repulsion forces between the micelles such as the oleyl ($\xi = 1.5$) solution, the chances for transient contacts between micelles are large making the second step more difficult [20,21]. For oleyl ($\xi = 1.5$) we were unable to perform experiments at high enough shear-rate to reach the second step.

For most solutions with threadlike micelles such as oleyl ($\xi = 1.0$), elaidyl ($\xi = 1.0$ and 1.5), the critical shear rate for the second step of the alignment process is lower and strong viscoelasticity of the solution in the form of non-zero N_1 is observed even at low shear rates. Surfactant solutions can exhibit drag reducing properties during both the first and the second alignment process. Based on the results with the elaidyl ($\xi = 2.5$) solution, surfactant solutions with significant numbers of branched threadlike micelles apparently can also exhibit strong viscoelasticity just like those with entangled threadlike micelles. Viscoelasticity of surfactant solutions is not vital for surfactant solutions to be drag reducing, however, as observed here with the oleyl ($\xi = 1.5$) solutions.

3.3.3. Apparent extensional viscosity and extensional/shear viscosity ratio

The apparent extensional viscosities of the oleyl and elaidyl surfactant solutions with different counterion/surfactant concentration ratios at room temperature are shown in Fig. 7. Their apparent extensional viscosities generally follow the same trends as their shear viscosities. At $\xi = 1$, the apparent extensional viscosities of the oleyl solution are much larger than those of the elaidyl ($\xi = 1$) solution at extensional rates less than 4000 s^{-1}. However, near 4000 s^{-1}, the apparent extensional viscosities of all but the elaidyl $\xi = 2.5$ solutions decrease and are very close to each other. The sharp drop in the apparent extensional viscosities of the solutions at high extensional rate may be caused by destruction of their micelle structures at very strong elongation [50,51] while the continued high values for elaidyl $\xi = 2.5$ are due to the high shear resistance of the branched micelles.

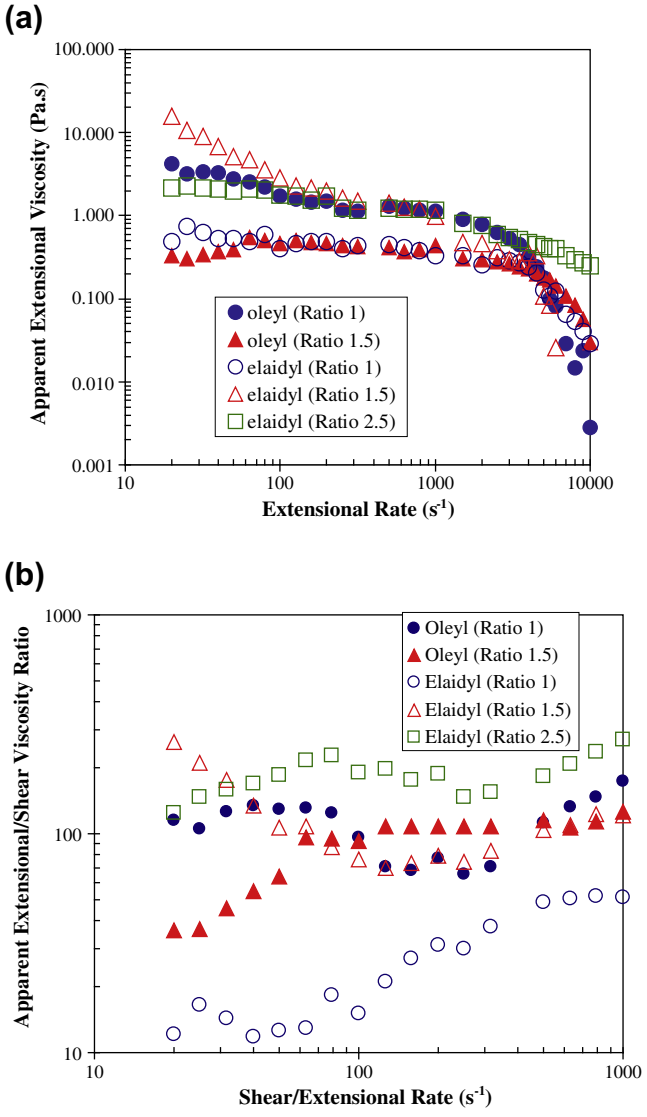

Fig. 7. (a) Apparent extensional viscosity; (b) apparent extensional/shear viscosity ratios of oleyl and elaidyl (5 mM)/sodium salicylate (5 mM; 7.5 mM and 12.5 mM) solutions at room temperature. *Note*: oleyl ($\xi = 2.5$) solution is insoluble until 50 °C.

At counterion/surfactant concentration ratio, $\xi = 1.5$, apparent extensional viscosities of the elaidyl solution are much greater than at $\xi = 1.0$, while those of the oleyl ($\xi = 1.5$) solution are near those of elaidyl at $\xi = 1.0$. This trend is similar to their low shear-rate shear-viscosity behaviors. As a result, the apparent extensional/shear viscosity ratios of the latter two solutions are close at apparent extensional/shear rates above 50 s^{-1}. Similar to the $\xi = 1.0$ solutions, sudden drops of apparent extensional viscosities of both solutions occur at extensional rates above 4000 s^{-1}.

For surfactant solutions oleyl ($\xi = 1.0$) and elaidyl ($\xi = 1.5$) which have long threadlike micelles or a mixture of long threadlike micelles and vesicles, relatively high apparent extensional viscosities are observed at extensional rates lower than the critical extensional rate of 4000 s^{-1} (where apparent extensional viscosity decreases dramatically) as shown in Fig. 7. High extensional viscosities are also found in the elaidyl ($\xi = 2.5$) solution with branched threadlike micelles.

The apparent extensional viscosities of elaidyl ($\xi = 1.0$) solution and oleyl ($\xi = 1.5$) solutions up to about 4000 s^{-1} are relatively low compared to the other solutions. The relatively low apparent extensional viscosity of the elaidyl ($\xi = 1.0$) solution may be caused by the shorter contour lengths of its micelles compared with those of the oleyl ($\xi = 1.0$) and elaidyl ($\xi = 1.5$) solutions, as discussed in the counterion concentration and alkyl chain configurations analysis in the cryo-TEM imaging section. For the oleyl ($\xi = 1.5$) solution, very flexible threadlike micelles with many curves between the entangling points of the micelles could be the cause of its relatively low apparent extensional viscosity.

3.4. ^{1}H NMR results

To better understand how differences in the drag-reduction and rheological behaviors of oleyl and elaidyltrimethylammonium chloride solutions, ^{1}H NMR studies of both oleyl and elaidyl trimethylammonium chloride surfactant solutions at different ξ were conducted, along with studies of the salicylate counterion in their presence. Based on chemical shift changes and line broadening observed at different ratios of surfactant to NaSal ($\xi = 0.4$–2.5), it was concluded that NaSal inserts into micelles of both the oleyl and elaidyl surfactants, however, the onset of micelle formation occurs at smaller values of ξ in the oleyl system than in the elaidyl system, indicating that the kinked hydrocarbon chain of the oleyl is more favorable for micelle growth than the elaidyl. A detailed discussion of these studies with NMR traces appears in Supporting information.

4. Summary

The first drag reduction, rheology and nanostructure comparisons of cationic surfactants with cis and trans chain configurations are reported here on (cis) oleyl trimethyl ammonium chloride vs. (trans) elaidyl trimethyl chloride with sodium salicylate counterion. This study demonstrated the following:

1. ^{1}H NMR studies of the two surfactants at different counterion/surfactant ratios show that salicylate penetrates into the hydrophobic center of the micelle with the 4-, 5-position protons intercalated inside the micelle while the 6-position proton remains in the polar environment. Addition of counterions gave broadening of both the surfactant and the salicylate proton signals indicating micelle size growth. At the same counterion/surfactant molar ratio, broadening is greater for the oleyl than the elaidyl surfactant, indicating that the kinked hydrocarbon chain configuration of the cis oleyl is more favorable for micelle growth than the trans elaidyl. The increased length and flexibility of the oleyl surfactant result in higher critical wall stress for breakup of micelles which causes decrease in turbulent drag reduction for this surfactant than for the elaidyl surfactant. This is due to reduced repulsive forces between the micelles (inter-micellar) and between micelle segments along the length of the micelle (intra-micellar) causing the cis micelles to be more robust than the trans.
2. Threadlike micelles in surfactant solutions are vital to the mechanism underlying turbulent drag reduction [5]. However, we show that it is not necessary for threadlike micelle nanostructures to be present in quiescent solution as shearing of vesicles can induce formation of effective drag reducing threadlike micelle structures
3. While the oleyl surfactant solution phase separates between $\xi = 1.0$–1.5 under quiescent conditions, it is solubilized by shear at $\xi = 1.5$ in turbulent flows, in rheological measurements and in the blotting step in cryo-TEM sample preparation.
4. Contrary to the assertions of many investigators (for example [5,10,52]) that viscoelasticity is a requirement for surfactant drag reduction, the drag reducing oleyl surfactant at $\xi = 1.5$ had zero N_1 and essentially no recoil.
5. Shear induced structures are observed only for surfactant systems having non-zero first normal stresses. While Nowak [48] stated that elastic effects coincide with sudden increase in viscosity and Qi et al. [49] stated that the shear rate for initiation of non-zero N_1 was near that of initiation of shear induced structure formation, here we note that for the elaidyl system, with $\xi = 1.0$, 1.5 and 2.5 and the oleyl at $\xi = 1.0$, non-zero N_1 values are initiated at shear rates below those observed for the initiation of shear induced structures.
6. All solutions that were effective drag reducers at room temperature also had high apparent extensional viscosities (greater or equal to 0–.3 Pa s). This supports the proposed drag reduction mechanism in which high extensional viscosity promotes stretching of the micelles and inhibits eddy formation in the near wall region [53,54].
7. Branched micelles formed in the elaidyl surfactant solution at high counterion/surfactant molar ratios had low viscosity and high critical wall shear stresses for destruction of the micelles and loss of drag reduction, Therefore, formulation of effective drag reducing cationic surfactant systems for use in industrial district heating and district cooling systems should be designed with high counterion/surfactant ratios to ensure desirable branched structures.

Acknowledgments

We thank the Petroleum Research Fund, administered by the American Chemical Society for partial financial support of the research. Y. Qi acknowledges the support of a University Fellowship and a Presidential Fellowship from The Ohio State University. NMR measurements were performed using a Bruker AM-600 600 MHz (14.14 T) NMR spectrometer at the OSU Campus Chemical Instrument Center by Dr. Charles Cottrell. The cryo-TEM work was performed at the Hannah and George Krumholz Advanced Microscopy Laboratory, part of the Technion Project of Complex Fluids, Microstructure and Macromolecules.

Appendix A. Supplementary material

The supporting information is available about NMR spectra and discussion supporting the summary provided in the text. Supplementary data associated with this article can be found, in the online version, at doi:10.1016/j.jcis.2010.10.067.

References

[1] J.L. Zakin, Y. Zhang, W. Ge, R. Zana, E.W. Kaler (Eds.), Giant Micelles: Properties and Applications, CRC Press/Taylor and Francis, New York, 2007.
[2] J.F. Motier, A.M. Carreir, Recent studies on polymer drag reduction in commercial pipelines, in: R. Sellin, R. Moses (Eds.), Drag reduction in Fluid Flows: Techniques for Friction Control, Ellis Horwood, West Sussex, UK, 1989, pp. 197–204.
[3] J.P. Rothstein, J. Rheol. 47 (5) (2003) 1227.
[4] Cates, Turner, Europkys. Lett. 11 (1990) 681.
[5] A. Gyr, H-.W. Bewersdorff, Drag Reduction of Turbulent Flows by Additives, Kluwer Academic Publishers, 1995.
[6] S. Tamano, M. Itoh, T. Inoue, K. Katom, K. Yokota, Phys. Fluids 21 (2009) 21.
[7] A. Gyr, J. Beihler, J. Non-Newtonian Fluid Mech. 165 (2010) 672.
[8] Y. Hu, E.F. Matthys, Rheol. Acta 34 (1995) 450.
[9] A. Krope, L.C. Lipus, Appl. Thermal. Eng. 30 (2010) 833.
[10] G.D. Rose, K.L. Foster, J. Non-Newtonian Fluid Mech. 31 (1989) 59.
[11] R.G. Laughlin, The Aqueous Phase Behavior of Surfactants, Academic Press, Harcourt Brace & Company, 1994.
[12] B. Lu, X. Li, J.L. Zakin, Y. Talmon, J. Non-Newtonian Fluid Mech. 71 (1997) 59.
[13] Dr. Sidney Shapiro, Akzo Nobel Research, Personal Communication.
[14] J. Israelachivili, Intermolecular and Surface Force, Academic Press, Harcourt Brace & Company, 1992.
[15] B. Lu, Characterization of Drag Reducing Surfactant Systems by Rheology and Flow Birefringence Measurements, The Ohio State University, Columbus, OH, 1997.
[16] C.W. Macosko, Rheology: Principles, Measurements, and Applications, VCH, New York, 1994.
[17] Y. Talmon, Ber. Bunsenges. Phys. Chem. 100 (1996) 364.
[18] Y. Talmon, R. Zana, E.W. Kaler (Eds.), Giant Micelles: Properties and Applications, CRC Press/Taylor and Francis, New York, 2007.
[19] Y. Zheng, Z. Lin, J.L. Zakin, Y. Talmon, L.T. Davis, L.E. Scriven, J. Phys. Chem. B 104 (2000) 5263.
[20] P.D. Butler, L.J. Magid, W.A. Hamilton, J.B. Hayter, B. Hammouda, P.J. Kreke, J. Phys. Chem. 100 (1996) 442.
[21] W.A. Hamilton, P.D. Butler, J.B. Hayter, L.J. Magid, P.J. Kreke, J. Phys. B (Amsterdam, Neth.) 221 (1996) 309.
[22] S.J. Candau, P. Hebraud, V. Schmitt, F. Lequeux, F. Kern, R. Zana, IL Nuovo Cimento 16D (9) (1994) 1401.
[23] L.J. Magid, Z. Han, Z. Li, P.V. Butler, J. Chem. Phys. B 104 (2000) 6717.
[24] L. Arleth, M. Bergstrom, Langmuir 18 (2002) 5343.
[25] V. Croce, T. Cosgrove, G. Maitland, T. Hughes, G. Karlsson, Langmuir 19 (2003) 8536.
[26] J.S. Pedersen, L. Cannavacciuola, P. Schurenberger, R. Zana, E.W. Kaler (Eds.), Giant Micelles: Properties and Applications, CRC Press/Taylor and Francis, New York, 2007.
[27] Y. Qi, J.L. Zakin, Ind. Eng. Chem. Res. 41 (2002) 6326.
[28] Z. Lin, Langmuir 12 (1996) 1729.
[29] F. Lequeux, S.J. Candau, Theoretical Challenges in the Dynamics of Complex Fluids, Kluwer Academic Publishers, 1997.
[30] R.D. Koehler, S.R. Raghavan, E.W. Kaler, Chem. Phys. B 104 (2000) 11035.
[31] S.R. Raghavan, H. Edmund, E.W. Kaler, Langmuir 18 (2002) 1056.
[32] S. May, A. Ben-Shaul, R. Zana, E.W. Kaler (Eds.), Giant Micelles: Properties and Applications, CRC Press/Taylor and Francis, New York, 2007.
[33] Y. Zhang, Correlations among Surfactant Drag Reduction, Additive Chemical Structures, Rheological Properties and Microstructures in Water and Water/co-solvent Systems, The Ohio State University, Columbus, OH, 2005.
[34] M. Chellamuthu, J.P. Rothstein, J. Rheol. (Melville, NY, US) 52 (2008) 865.
[35] A. Khatory, F. Kern, F. Lequeux, J. Appell, G. Porte, N. Morie, A. Ott, W. Urbach, Langmuir 9 (1993) 933.
[36] D. Danino, Y. Talmon, H. Levy, G. Beinert, R. Zana, Science 269 (1995) 1420.
[37] M.E. Cates, J. Phys.: Condens. Matter 8 (1996) 9167.
[38] P.A. Hassan, S.J. Candau, F. Kern, C. Manohar, Langmuir 14 (1998) 6025.
[39] T.J. Drye, M.E. Cates, J. Chem. Phys. 96 (1992) 1367.
[40] F. Lequeux, Curr. Opin. Colloid Interface Sci. 1 (1996) 341.
[41] T. Shikata, Y. Morishima, Langmuir 13 (1997) 1931.
[42] S. Hofmann, H. Hoffmann, J. Phys. Chem. B 102 (1998) 5614.
[43] M.E. Cates, M.S. Turner, Europhys. Lett. 11 (1990) 681.
[44] M.S. Turner, M.E. Cates, J. Phys.: Condens. Matter 4 (1992) 3719.
[45] M.E. Cates, Philos. Trans. R. Soc., A 344 (1993) 339.
[46] H. Rehage, H. Hoffmann, J. Phys. Chem. 92 (1988) 4712.
[47] R. Cressely, V. Hartmann, Eur. Phys. J. B 6 (1998) 57.
[48] M. Nowak, Rheol. Acta 40 (2001) 366.
[49] Y. Qi, K. Littrell, P. Thiyagarajan, Y. Talmon, J. Schmidt, Z. Lin, J.L. Zakin, J. Colloid Interface Sci. 337 (2009) 218.
[50] K. Vissmann, H.W. Bewersdorff, J. Non-Newtonian Fluid Mech. 34 (1990) 289.
[51] R.K. Prud'homme, G.G. Warr, Langmuir 10 (1994) 3419.
[52] J.C. Savins, Rheol. Acta 6 (1967) 323.
[53] J. Hoyt, in: J. Kroschwitz, H.F. Mark, N.M. Bikales, C.G. Overberge, G. Menges (Eds.), Drag Resuction 1986 in Encyclopedia of Polymer Science and Engineering, vol. 5, Wiley, New York, 1986.
[54] H.-W. Bewersdorf, A. Gyr, K. Hoyer, A. Tsinober, Rheol. Acta 32 (1993) 140.